Modelling and estimation of the cardiac electromechanical activity

J. Sainte-Marie, R. Cimrman, M. Sorine and D. Chapelle

5th July 2004

Contents

* * * * * * * * *

1 Presentation

The knowledge of the heart behavior and the power of data acquisition techniques (ECG, ultrasound or MRI images,...) have greatly improved during the last decades. In-vivo measurements of the cardiac activity are very valuable for clinical purposes, but some crucial biological quantities are hardly – or not at all – accessible, as e.g. for stresses / pressures or constitutive parameters that may reflect pathologies. In order to reach these quantities *modeling* is required. On the other hand the complexity and diversity of the physical phenomena involved in the heart behavior are a major challenge for modeling. In particular the various data (constitutive parameters, boundary conditions, and so on) necessary to perform accurate simulations of the models cannot be determined *a priori*.

The work presented in this document has two objectives. The first is to build and validate a 3D simulator of the electromechanical activity of the myocardium. The simulator is calibrated using measurements and classical outputs of the cardiac activity and some importants parameters of the model can be fitted by the user. Typically, the local excitability and contractility of the muscle can be adjusted to simulate pathological behaviors.

The second objective is to "couple" the validated model with the *in vivo* measurements of the cardiac activity of a patient with a view to helping clinicians to diagnose heart pathologies. Some of the parameters used in

the electromechanical model are crucial for medical purposes and the approach we propose aims at using measurements of the cardiac activity in order to perform an identification of the parameters and state of the global electromechanical heart model, hence to give access to quantities of interest for diagnosing activation and contraction troubles.

This work has been carried out in the framework of the multidisciplinary research project ICEMA (Images of the Cardiac ElectroMechanical Activity, see [4, 31]) involving several research teams at INRIA, other academic institutions and Philips Research France. In this paper, we focus on the mechanical model, the electromechanical coupling and the simulation of a heart cycle; the electrical activity modeling is not considered and for the simulations, we use given propagating action potentials with possibly added perturbations. The coupling of the 3D electromechanocal model with a data assimilation procedure is shortly presented at the end of this paper and a future paper will be devoted to this promising approach.

This paper is divided into four parts. The 3D excitation-contraction model and especially the constitutive law of the myofibril inserted in the rheological model are first presented. The second section is devoted to the implementation of the obtained model. In section 4, simulations of healthy and pathological heart cycles are presented. Finally, the formulation of the data assimilation technique for the proposed model in order to achieve state/parameter estimation is desribed and preliminary results are given.

2 The 3D heart model

The necessary ingredients to obtain a 3D electromechanical model of the myocardium are the following

- a constitutive law for the active and passive behavior of the fibres,
- the electrical activation that can be obtained fron numerical simulations of simplified or more complex modeling of the action potential propagation,
- a geometrical model of the myocardium with the fibres directions,
- realistic boundary conditions for the muscle,
- a model for the valve opening and closure in order to distinguish the isovolumetric phases from the non-isovolumetric phases and also a model for the blood.

Each of these components is described in this section.

2.1 A constitutive law for the myofibres

It is commonly admitted that the model of actin-myosin bridge dynamics due to Huxley [17] allows to describe the muscle contraction phenomena on the sarcomere scale. Furthermore, Zahalak [41] has shown how the method of moments can be applied to this model in order to describe muscle-contraction on the myofibre scale. However, most modeling endeavours still rely on heuristic approaches and experimental testing, whether directly at the macroscopic level [16], or in order to identify the attachment and detachment rates of the bridges [40].

We have designed a chemically-controlled constitutive law of cardiac myofibre mechanics introduced in [5] and consistent with the behavior of myosin molecular motors [18]. The resulting sarcomere dynamics – derived by applying the moment-scaling method with the first two moments corresponding to active stiffness and stress, see [5] – is in agreement with the "sliding filament hypothesis" introduced in [17]. With a particular choice of the attachment and detachment rates, it is compatible in particular with Hill's force-velocity relation, visco-elastic passive behavior and active relaxation descriptions.

Denoting by σ_c the active stress and by ε_c the strain along the sarcomere, the relation between σ_c and ε_c is given by the following set of ordinary differential equations:

$$\begin{cases} \dot{\tau}_c = k_c\dot{\varepsilon}_c - (\alpha|\dot{\varepsilon}_c| + |u|)\tau_c + \sigma_0|u|_+ & \tau_c(0) = 0 \\ \dot{k}_c = -(\alpha|\dot{\varepsilon}_c| + |u|)k_c + k_0|u|_+ & k_c(0) = 0 \\ \sigma_c = \tau_c + \mu_c\dot{\varepsilon}_c + k_c\xi_0 \end{cases} \tag{1}$$

where u denotes the electrical input, with $u > 0$ during contraction and $u < 0$ during active relaxation. The parameters k_0 and σ_0 are related with the maximum available actin-myosin cross-bridges in the sarcomere and μ_c is a viscosity parameter. The rate at which the cross-bridges unfasten during passive relaxation is given by $\alpha|\dot{\varepsilon}_c|$, and during active relaxation by $|u|+\alpha|\dot{\varepsilon}_c|$.

2.1.1 The Starling effect

The Starling mechanism is one of the most important regulatory mechanisms that allows the heart to regulate its activity. When the preload increases, the heart is able to increase its contraction. The preload corresponds to the initial stretching of the cardiac fibres at the end of the diastolic filling, so

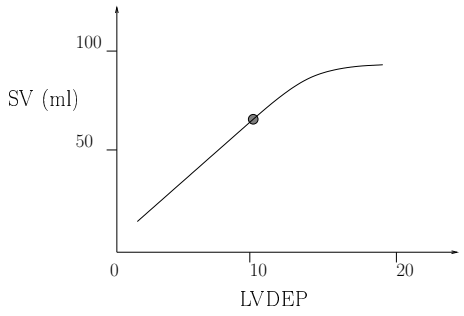

Figure 1: The Franck-Starling curve (SV: stroke volume, LVDEP: left ventricular end-diastolic pressure).

one can relate the preload to the veinous return and the auricular pressure. In summary, increasing the ventricular end diastolic pressure leads to an increase in the stroke volume, see Fig. 1. The Starling effect can also be formulated saying the heart adapts its contraction so that the stroke volume equals the end-diastolic volume.

The underlying physiological mecanism is the following: when the stretching of the sarcomere increases, the troponin C calcium sensitivity also increases leading to a growth of the cross-bridge attachment availability. This means that when the stretching of the sarcomere increases we move from (a) to (b) on the curve presented in Fig. 2-(i), note that the normal range for the sarcomere length is denoted by I. This phenomenon is no more valid for large strains of the sarcomere. The case (b) also depicted in Fig. 3 corresponds to a normal deformation of the sarcomere whereas (a) and (c) corresponds to large deformation (negative and positive). It appears that for large deformation less actin-myosin cross-bridges can be created. This leads to the modified constitutive law given by (2) where $d(\varepsilon_c)$ behaves like the function presented in Fig. 2-(ii).

$$\begin{cases} \dot{\tau}_c = k_c\dot{\varepsilon}_c - (\alpha|\dot{\varepsilon}_c| + |u|)\tau_c + \sigma_0|u|_+ & \tau_c(0) = \tau_{c_0} \\ \dot{k}_c = -(\alpha|\dot{\varepsilon}_c| + |u|)k_c + k_0|u|_+ & k_c(0) = k_{c_0} \\ \sigma_c = d(\varepsilon_c)(\tau_c + k_c\xi_0) + \mu_c\dot{\varepsilon}_c \end{cases} \tag{2}$$

2.1.2 Thermomechanical compatibility

The stress in the myofibre is given by σ_c, output of the system (2). Since $0 \leq k_c(0) \leq k_0$, Eq. (2-b) ensures $0 \leq k_c \leq k_0$ so k_c can be seen as the progress of the chemical reaction (ATP hydrolysis) governing the creation of

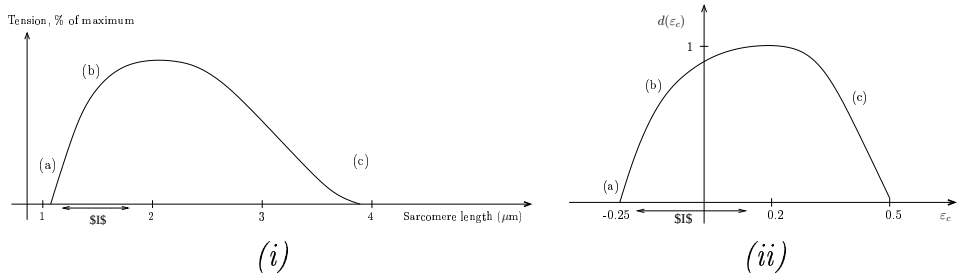

Figure 2: *(i)* the "length-tension" curve of a muscle with the three different configurations of the sarcomere given in Fig. 3 and *(i)* the corresponding modulation $d(\varepsilon_c)$ of the active stress σ_c.

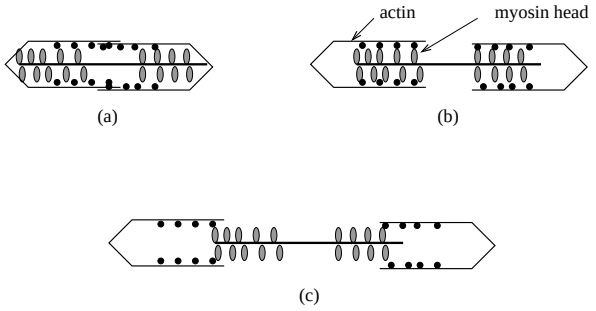

Figure 3: Three different sarcomere deformations.

the cross-bridges. For small k_c, few cross-bridges are fastened whereas for $k_c \approx k_0$ the majority of the actin-myosin bridges are attached.

Let us introduce the new variable v defined by

$$v = |u| + \alpha|\dot{\varepsilon}_c|$$

that is analogous to a time rate. Then the first equation of (2) can be rewritten under the form

$$\dot{\tau}_c = v\left(\frac{k_c\dot{\varepsilon}_c + \sigma_0|u|_+}{v} - \tau_c\right) \tag{3}$$

and under this form, two contributions appears in τ_c; one coming from the chemical input u and the other one from the internal deformation variable ε_c. If we suppose $\dot{\varepsilon}_c$ is bounded with $|\dot{\varepsilon}_c| \leq a$ then σ_c is also bounded. Actually, using (3) one has

$$|\tau_c| \leq \sup_t \frac{k_c\dot{\varepsilon}_c + \sigma_0|u|_+}{\alpha|\dot{\varepsilon}_c| + |u|} \leq \sigma_0 + \frac{k_0}{\alpha}$$

leading to $|\sigma_c| \leq \frac{k_0}{\alpha} + \mu_c a$.

Considering the variable $\tilde{\tau}_c = \tau_c + k_c\xi_0$, system (2) can be written under the form

$$\begin{cases} \dot{\tilde{\tau}}_c = k_c\dot{\varepsilon}_c - (\alpha|\dot{\varepsilon}_c| + |u|)\tilde{\tau}_c + (\sigma_0 - k_0\xi_0)|u|_+ & \tilde{\tau}_c(0) = \tau_{c_0} + k_{c_0}\xi_0 \\ \dot{k}_c = -(\alpha|\dot{\varepsilon}_c| + |u|)k_c + k_0|u|_+ & k_c(0) = k_{c_0} \\ \sigma_c = d(\varepsilon_c)\tilde{\tau}_c + \mu_c\dot{\varepsilon}_c \end{cases}$$

meaning that a convenient choice of σ_0 allows to consider $\xi_0 = 0$. So in the following we consider the constitutive law is given by (2) with $\xi_0 = 0$. We introduce the new variable ε_c^e defined by $\tau_c = k_c\varepsilon_c^e$ and that could be seen as the elastic part of ε_c. Then replacing the expression of ε_c^e into the first equation of (2) leads to

$$\dot{\varepsilon}_c^e = \dot{\varepsilon}_c + \frac{\sigma_0}{k_c}|u|_+ - \frac{k_0}{k_c}|u|_+\varepsilon_c^e. \tag{4}$$

Now let us define $\varepsilon_c = \varepsilon_c^e + \varepsilon_c^p$ then ε_c^p satisfies

$$\dot{\varepsilon}_c^p = -\frac{\sigma_0}{k_c}|u|_+ + \frac{k_0}{k_c}|u|_+(\varepsilon_c - \varepsilon_c^p). \tag{5}$$

Neglecting the Starling effect i.e. $d(\varepsilon_c) = 1$, the mechanical power of system (2) defined by $\sigma_c\dot{\varepsilon}_c$ can be written under the form

$$\begin{aligned} \sigma_c\dot{\varepsilon}_c &= \frac{\partial\left(\frac{k_c}{2}(\varepsilon_c^e)^2\right)}{\partial t} + \mu_c\dot{\varepsilon}_c^2 + k_c\varepsilon_c^e\dot{\varepsilon}_c^p - \dot{k}_c\frac{(\varepsilon_c^e)^2}{2} \\ &= \frac{\partial\left(\frac{k_c}{2}(\varepsilon_c^e)^2\right)}{\partial t} + \mu_c\dot{\varepsilon}_c^2 + k_c\varepsilon_c^e\dot{\varepsilon}_c^p + \frac{(\varepsilon_c^e)^2}{2}((\alpha|\dot{\varepsilon}_c| + |u|)k_c - k_0|u|_+) \end{aligned}$$

and using (5) it comes

$$k_c\varepsilon_c^e\dot{\varepsilon}_c^p = k_0|u|_+(\varepsilon_c^e)^2 - \sigma_0|u|_+\varepsilon_c^e.$$

So finally the mechanical power is

$$\sigma_c\dot{\varepsilon}_c = \frac{\partial\left(\frac{k_c}{2}(\varepsilon_c^e)^2\right)}{\partial t} + \mu_c\dot{\varepsilon}_c^2 + \frac{(\varepsilon_c^e)^2}{2}\left(k_0|u|_+ + (\alpha|\dot{\varepsilon}_c| + |u|)k_c\right) - \sigma_0|u|_+\varepsilon_c^e \quad (6)$$

In the absence of external excitation ($u \equiv 0$) we have the following thermo-mechanical interpretation: $\frac{\partial\ \frac{1}{2}k_c(\varepsilon_c^e)^2}{\partial t}$ appears as a free energy and $\mu_c\dot{\varepsilon}_c^2 + \alpha|\dot{\varepsilon}_c|k_c\frac{(\varepsilon_c^e)^2}{2}$ appears as a nonegative pseudo-potential of dissipation so the second principle of thermodynamics is satisfied. Since $\varepsilon_c^e = \frac{\tau_c}{k_c}$, rewritting (6) as

$$\sigma_c\dot{\varepsilon}_c - \frac{\partial\left(\frac{\tau_c^2}{2k_c}\right)}{\partial t} = \mu_c\dot{\varepsilon}_c^2 + \frac{(\tau_c)^2}{2k_c}(\alpha|\dot{\varepsilon}_c| + |u|) + \left(\frac{k_0}{2}\frac{\tau_c^2}{k_c^2} - \sigma_0\frac{\tau_c}{k_c}\right)|u|_+$$

it appears that energy can be supplied to the system only if $u > 0$ and $0 < \tau_c \leq 2\sigma_0\frac{k_c}{k_0}$.

Taking into account the Starling effect, the previous equality becomes

$$\begin{aligned}\sigma_c\dot{\varepsilon}_c - \frac{\partial\left(d(\varepsilon_c)\frac{\tau_c^2}{2k_c}\right)}{\partial t} = \mu_c\dot{\varepsilon}_c^2 + \frac{d(\varepsilon_c)(\tau_c)^2}{2k_c}(\alpha|\dot{\varepsilon}_c| + |u|) \\ + d(\varepsilon_c)\left(\frac{k_0}{2}\frac{\tau_c^2}{k_c^2} - \sigma_0\frac{\tau_c}{k_c}\right)|u|_+ - \dot{\varepsilon}_c\dot{d}(\varepsilon_c)\frac{\tau_c^2}{2k_c} \quad (7)\end{aligned}$$

2.2 The electrical activation

The propagation of the action potential u activating the muscle contraction can be modelled by nonlinear reaction-diffusion equations [24]. For complementary informations, one can refer to the works of Hodgkin and Huxley [1] or the simpler FitzHugh-Nagumo model [12]. For our simulations we have mainly used the two-variable FitzHugh-Nagumo model proposed by Aliev and Panfilov [2].

The membrane potential variations in one point of the myocardium along a cardiac cycle can be represented by the curve in Fig. 4. We consider the Ca^{2+} concentration within the cardiac cells allows the creation of cross-bridges only when the menbrane potential is greater then MP_{lim}. This means the

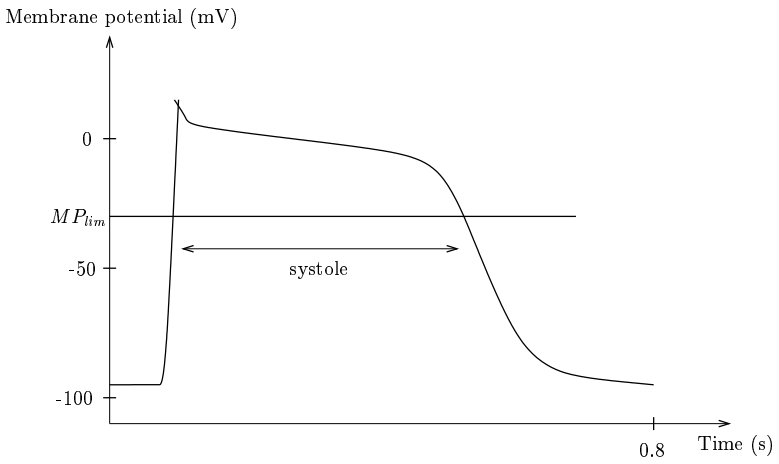

Figure 4: Membrane potential along a cardiac cycle.

membrane potential and the input u in the constitutive law (2) are related by:

$$u(t) = MP(t) - MP_{lim}.$$

For the simulations presented at the end of this document, several types of activations have been used:

- a uniform activation i.e. no propagation of the action potential (for all points M of the muscle $u(M,t) = u(t)$).
- A simplified propagation is considered with $u(M,t) = MP(t - \frac{\Pi_z M}{V}) - MP_{lim}$ where $\Pi_z M$ is the projection of M along the apex to base axis and V is the speed of the wave front.
- The membrane potential is simulated using the FitzHugh-Nagumo equations [12].

In each case, the effects of the mechano-electric feedback are not considered.

2.3 The rheological model

The myofibre constitutive law described above is now incorporated in a rheological model of Hill-Maxwell type [6, 14], as depicted in Fig. 5-a. The element E_c accounts for the contractile electrically-activated behavior governed by (1) and each variable appearing with index c refers to this element.

An elastic material law is used for the series element E_s and a visco-elastic one is used for E_p. Based on experimental results, the corresponding stress-strain laws are generally assumed to be of exponential type for E_p [38], and linear for E_s [29]. The role of E_p is to prevent the heart from overstepping certain limits during filling or ejection, while E_s and E_c allow the contraction and the active relaxation.

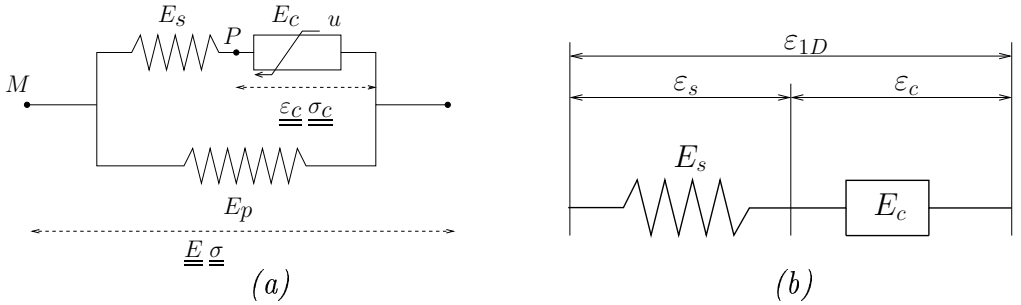

Figure 5: *(a)* Hill-Maxwell rheological model and *(b)* strains in the active branch.

The composition of deformations in the active branch is described in Fig. 5-b. It follows from thermodynamical considerations that $1+\varepsilon_{1D} = (1+\varepsilon_c)(1+\varepsilon_s)$ while the generated tension σ_{1D} is

$$\sigma_{1D} = \frac{\sigma_c}{1+\varepsilon_s} = \frac{\sigma_s}{1+\varepsilon_c}. \tag{8}$$

Let us denote $\underline{n}$ the direction of the cardiac fibre in the myocardium and $\underline{\underline{E}}$ the Green-Lagrange strain tensor then one has

$$\varepsilon_{1D} = \sum_{i,j} E_{ij} n_i n_j. \tag{9}$$

2.4 Description of the parallel branch

In paragraph 2.1 we have described the contractile element, we now focus on the parallel element E_p. Assuming we consider an isothermal process, the satisfaction of the Clausius-Duhem inequality [37] when no dissipation is considered leads to

$$\underline{\underline{\sigma_p^e}} = 2\rho_0 \frac{\partial W^e}{\partial \underline{\underline{E}}}$$

ρ_0 being the density expressed in the reference state and W^e an elastic strain energy potential. When viscosity is added, the Clausius-Duhem inequality

becomes

$$\left(\underline{\underline{\sigma_p}} - 2\rho_0 \frac{\partial W^e}{\partial \underline{\underline{E}}}\right) : \underline{\underline{\dot{E}}} \geq 0 \qquad \forall \underline{\underline{E}}, \underline{\underline{\dot{E}}}$$

and a viscous pseudo-potential $W^v(\underline{\underline{E}}, \underline{\underline{\dot{E}}})$ accounting for energy dissipation ought to satisfy

$$\frac{\partial W^v}{\partial \underline{\underline{\dot{E}}}} : \underline{\underline{\dot{E}}} \geq 0 \qquad \forall \underline{\underline{\dot{E}}}. \tag{10}$$

Equation (10) holds true when the potential W^v is continuous, positive and convex. Moreover the value of W^v must be zero when the strain rate equals zero [10]. Therefore, the components of the passive stress $\underline{\underline{\sigma_p}}$ are defined by

$$\begin{aligned} \underline{\underline{\sigma_p}}(\underline{\underline{E}}, \underline{\underline{\dot{E}}}) &= 2\rho_0 \frac{\partial W^e}{\partial \underline{\underline{E}}} + \frac{\partial W^v}{\partial \underline{\underline{\dot{E}}}} \\ &= \sigma_p^e(\underline{\underline{E}}) + \sigma_p^v(\underline{\underline{E}}, \underline{\underline{\dot{E}}}) \end{aligned}$$

Two strain energy functions satisfying the thermomechanical compatibility are typically used in the litterature leading to Mooney-Rivlin materials and Veronda-Westmann materials [13, 15, 22, 38]. Following this, W^e appears as a linear combination of the following terms

$$\begin{array}{lll} W_1^e = \kappa_1(\tilde{I}_1 - 3) & \ldots & \text{neo-Hookean term} \\ W_2^e = \kappa_2(\tilde{I}_2 - 3) & \ldots & \text{Mooney-Rivlin term} \\ W_3^e = \kappa_3(e^{\eta(\tilde{I}_1 - 3)} - 1) & \ldots & \text{Veronda-Westmann term} \end{array} \tag{11}$$

with the classical reduced invariants $\tilde{I}_1 = I_1 J^{-\frac{2}{3}}$, $\tilde{I}_2 = I_2 J^{-\frac{4}{3}}$. The elastic potential has to fulfill two different types of constraints: first the conditions ensuring a correct formulation of the problem i.e. the thermomechanical compatibility and the existence/uniqueness of the solution for the associated boundary value problem. Second, to be admissible an elastic potential must fit with experimental stress-strain curves. Following [32] and [38] we have mainly used the two following elastic strain energy functions

$$W^e = \kappa_1(\tilde{I}_1 - 3) + \kappa_2(\tilde{I}_2 - 3) \quad \text{and} \quad W^e = \kappa_3(e^{\eta(\tilde{I}_1 - 3)} - 1) - \frac{\kappa_3 \eta}{2}(\tilde{I}_2 - 3).$$

For the viscous potential W^v, we follow Pioletti *et al.* [33] and we use

$$W^v = \eta \mathrm{Tr}\,(\underline{\underline{\dot{C}}})^2 (I_1 - 3)$$

where $\underline{\underline{C}}$ is the right Cauchy-Green deformation tensor defined by $C_{ij} = 2E_{ij} + \delta_{ij}$. The calibration of the parameters appearing in W^e and W^v will

be discussed in paragraph 4.1. It has to be noticed that several authors do not restrict the choice of the constitutive law to those satisfying the mechanical constraints and prefer to ensure only a good stress-strain curve fitting with the experimental data. The most widely used experimental based strain energy function is called "pole-zero" and has been introduced by Hunter [34, 30], an alternative to the "pole-zero" law is given by Lin [26]. The preceding remark concerning the design of the constitutive law for passive fibres also holds for active fibres, see [40].

The model enables that at any material point both the passive and the active fibres can be defined in several preferential directions, as required by the histological observations. Since we do not use the mixed formulation, we considering the tissue is not purely incompressible and if $\underline{\underline{\sigma}}$ denotes the second Piola-Kirchhoff stress tensor, it comes

$$\underline{\underline{\sigma}} = -pJ\underline{\underline{C}}^{-1} + \sigma_p^e(\underline{\underline{E}}) + \sigma_p^v(\underline{\underline{E}}, \dot{\underline{\underline{E}}}) + \sigma_{1D}\ \underline{n} \otimes \underline{n} \tag{12}$$

where the first term corresponds to the volumetric behavior with $p = -K(J-1)$, K being the bulk modulus. $\sigma_p^e(\underline{\underline{E}})$ (elastic part of E_p) and $\sigma_p^v(\underline{\underline{E}}, \dot{\underline{\underline{E}}})$ (viscous part of E_p) accounts for the stresses in the parallel branch have been described above and $J = \det(\underline{\underline{F}})$ where $\underline{\underline{F}}$ is the deformation gradient.

Using Eqs. (2), (8), (9) and (12), the corresponding complete governing 3D mechanical equations, presented in [6], are given by the following set of equations

$$\begin{cases} \rho\ddot{\underline{y}} - \mathrm{div}(\underline{\underline{F}} \,.\, \underline{\underline{\sigma}}) = 0 \\ \underline{\underline{\sigma}} = -pJ\underline{\underline{C}}^{-1} + \sigma_p(\underline{\underline{E}}, \dot{\underline{\underline{E}}}) + \sigma_{1D}\ \underline{n} \otimes \underline{n} \\ \sigma_{1D} = \frac{\sigma_c}{1+\varepsilon_s} = \frac{\sigma_s}{1+\varepsilon_c} \\ \dot{\tau}_c = k_c\dot{\varepsilon}_c - (\alpha|\dot{\varepsilon}_c| + |u|)\tau_c + \sigma_0|u|_+ \\ \dot{k}_c = -(\alpha|\dot{\varepsilon}_c| + |u|)k_c + k_0|u|_+ \\ \sigma_c = d(\varepsilon_c)(\tau_c + k_c\xi_0) + \mu_c\dot{\varepsilon}_c \\ \sigma_s = E_s[(\varepsilon_{1D} - \varepsilon_c)/(1+\varepsilon_c)] \\ \varepsilon_{1D} = \sum_{i,j} E_{ij}n_in_j. \end{cases} \tag{13}$$

2.5 Coupling with the arteries and the atria

The successive phases of the cardiac cycle are distinguished in the coupling conditions between the ventricle and other parts of the cardiovascular system. With P_{v} denoting the blood pressure in a ventricle, P_{ar} the pressure in the corresponding artery and P_{at} the pressure in the atrium, the ejection occurs when $P_{\mathrm{v}} \geq P_{\mathrm{ar}}$ whereas the mitral valve opens when $P_{\mathrm{v}} \leq P_{\mathrm{at}}$, see Fig. 7-a.

2.5.1 The phases of the cardiac cycle

As already mentioned the cardiac cycle contains four successive phases, the isovolumetric contraction and the ejection during the systole, the isovolumetric relaxation and the filling during the diastole. From a mechanical point of view, the formulations of the complete problem arising during the isovolumetric phases and the non-isovolumetric phases are distinct. Let us consider problem (13) written in a shortened form

$$\rho\ddot{\underline{y}} - \mathrm{div}(\underline{\underline{F}} \cdot \underline{\underline{\sigma}}) = 0 \tag{14}$$

if at time t, $\Gamma^{(t)}$ denotes the surface of the ventricular cavity and $\Lambda^{(t)}$ its interior then the volume $V^{(t)}$ of each ventricle is defined by

$$V^{(t)} = \int_{\Lambda^{(t)}} dV \tag{15}$$

and using the Ostrogradski theorem it comes

$$V^{(t)} = \frac{1}{3} \int\limits_{\Gamma^{(t)}} x_i n_i^{(t)} \mathrm{d}\Gamma^{(t)} \tag{16}$$

where $\underline{x} = \underline{X} + \underline{y}$ are the actual coordinates and $\underline{n}^{(t)}$ points out of the cavity. Using (15), one can write

$$\dot{V}^{(t)} = \int\limits_{\Gamma^{(t)}} \dot{y}_i n_i^{(t)} \mathrm{d}\Gamma^{(t)} = D(\dot{y})$$

and during isovolumetric phases, problem (14) becomes

$$\left\{ \begin{array}{l} \rho\ddot{\underline{y}} - \mathrm{div}(\underline{\underline{F}} \cdot \underline{\underline{\sigma}}) = 0 \\ (\underline{\underline{F}}.\underline{\underline{\sigma}}).\underline{n} = -P_{\mathrm{v}}\ \underline{n} \quad \text{on} \ \ \Gamma^{(t)} \\ \dot{V}^{(t)} = D(y, \dot{y}) = 0 \end{array} \right. \tag{17}$$

P_{v} being the Lagrange multiplier of the volume conservation i.e. $\dot{V}^{(t)} = 0$. By contrast during the ejection and the filling, the boundary condition of problem (14) can be written in the form

$$\left\{ \begin{array}{l} (\underline{\underline{F}}.\underline{\underline{\sigma}}).\underline{n} = -P_{\mathrm{v}}\ \underline{n} \quad \text{on} \ \ \Gamma^{(t)} \\ P_{\mathrm{v}} = P_{\mathrm{ext}} \end{array} \right. \tag{18}$$

with P_{ext} equals P_{ar} or P_{at}. Due to numerical considerations the isovolumetric criterion (17-b) and (17-c) is transformed into a penalization problem under the form

$$\begin{cases} (\underline{\underline{F}}.\underline{\underline{\sigma}}) \,.\, \underline{n} = -P_{\text{v}} \quad \text{on } \Gamma^{(t)} \\ P_{\text{v}} = \lambda \dot{V}^{(t)} \end{cases}$$

with $\lambda \gg 1$. When modeling a cardiac cycle, the interaction between the blood and the intraventricular cavities corresponding to the equilibrium equation

$$(\underline{\underline{F}}.\underline{\underline{\sigma}}) \,.\, \underline{n} = -P_{\text{v}}\, \underline{n}$$

in (17) and (18) has to be considered. Because of the computational costs induced by taking into account a distributed flow model, the inertial effects of the fluid-structure interaction are neglected thus reducing the interaction force to the effects of blood pressure in each ventricle. For the moment we consider the blood in each ventricle is completely characterized by a uniform pressure P_{v} and the cavity volume V_{v}.

2.5.2 Valves opening and closure

The valves are not modelled using a distributed model but adding constraints on the volume variations of each ventricle. This is achieved by the means of an analogy with a double contact problem.

Let us consider two solids S_1 and S_2, the distance and the contact force between them are denoted d and F respectively. If there is contact between S_1 and S_2 then $d = 0$, if not then $F = 0$ so that these two situations are summarized by $Fd = 0$.

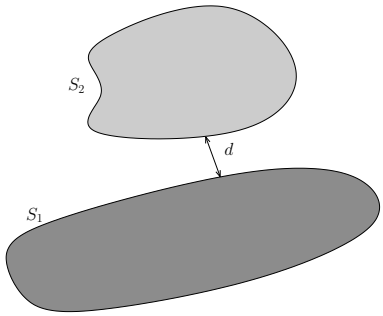

Figure 6: Contact between two solids.

The coupling conditions between a ventricle and the corresponding artery can be formulated similarly, the blood flow leaving each ventricle $Q = -\dot{V}$

being defined by $Q|P_{\rm v} - P_{\rm at}|_+$. Also considering the atrium, one obtains

$$\begin{cases} Q \geq 0 & \text{when } P_{\rm v} = P_{\rm ar} \quad \text{(ejection)} \\ Q = 0 & \text{when } P_{\rm at} < P_{\rm v} < P_{\rm ar} \quad \text{(isovol. phases)} \\ Q \leq 0 & \text{when } P_{\rm v} = P_{\rm at} \quad \text{(filling)}. \end{cases} \tag{19}$$

This formulation fully describes the blood flows through the valves but, since relation (19) is not regular, its discretization leads to numerical difficulties and a regularized version is needed (Fig. 7-b). The regularized version must satisfy the condition $\frac{dQ}{dP_{\rm v}} \geq 0$. We consider during the ejection, the blood flow is proportional to the difference of pressure $P_{\rm v} - P_{\rm ar}$ (see [28]) leading to

$$Q \approx K_{\rm ar}(P_{\rm v} - P_{\rm ar}) \tag{20}$$

with $K_{\rm ar} = \frac{\pi R^2}{\rho c}$, R being the radius of valve, ρ the blood density and c the velocity of wave propagation. Relation (20) written under the form $P_{\rm v} \approx P_{\rm ar} + \frac{Q}{K_{\rm ar}}$ is analogous to (18-b) where a small resistance due to the valve diameter is added. During the filling one has similarly $Q \approx K_{\rm at}(P_{\rm v} - P_{\rm at})$ so the regularized version of (19) is

$$\begin{cases} Q = e^{l_1(P_{\rm v}-P_{\rm ar})} - e^{l_2(P_{\rm at}-P_{\rm v})} & \text{when } P_{\rm at} - \delta_1 \leq P_{\rm v} \leq P_{\rm ar} + \delta_0 \\ Q = K_{\rm ar}(P_{\rm v} - P_{\rm ar}) + Q_0 & \text{when } P_{\rm v} \geq P_{\rm ar} + \delta_0 \\ Q = K_{\rm at}(P_{\rm v} - P_{\rm at}) + Q_1 & \text{when } P_{\rm v} \leq P_{\rm at} - \delta_1 \end{cases} \tag{21}$$

where Q_0 and Q_1 ensure Q is continuous and differentiable with respect to its variable and (δ_0, δ_1) are chosen small enough. Thus the pressure $P_{\rm v}$ in a ventricle is related to the change of volume of the considered ventricle using (21) i.e.

$$-\dot{V}_{\rm v} = Q = f(P_{\rm v}, P_{\rm ar}, P_{\rm at}). \tag{22}$$

When considering the left ventricle $(P_{\rm v}, P_{\rm ar}, P_{\rm at})$ corresponds to $(P_{\rm lv}, P_{\rm ao}, P_{\rm at,l})$ and similarly for the right ventricle $(P_{\rm v}, P_{\rm ar}, P_{\rm at})$ becomes $(P_{\rm rv}, P_{\rm ap}, P_{\rm at,r})$.

2.5.3 Windkessel model

To obtain a realistic pressure-volume response of the model, it is necessary to model the external blood circulation and thus to consider that $P_{\rm ar}$ vary along the cardiac cycle and especially during the ejection. For this it is possible to consider that $P_{\rm ar}$ follows a 0D windkessel type model or a 1D model of the blood flow. Up to now, the use of a 3D model of blood flow in arteries is out of reach. A simplified 1D model coupled with the heart model has been tested, the results are not presented in this article and will be published in a future paper.

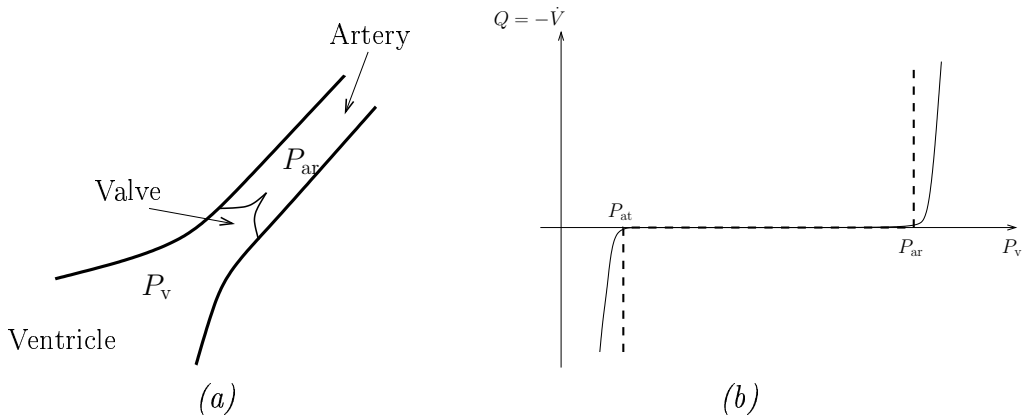

Figure 7: Aortic valve model, *(a)* mechanism and *(b)* formulation as a double contact problem, (- -) relation (19) and (–) relation (21).

Windkessel and similar lumped models are often used to represent blood flow and pressure in the arteries. These models can be derived from electrical circuit analogies where current represents arterial flow and voltage represents arterial pressure. The idea for the windkessel model was originally proposed by S. Hales in 1733 and further developed by O. Frank in 1899. For more informations about Windkessel models of blood flow in arteries, one can refer to [3, 39, 35].

The 4-element Windkessel model is governed by:

$$C\dot{P}_{\rm ar} + \frac{P_{\rm ar} - P_{\rm sv}}{R_p} = (1 + \frac{R_c}{R_p})|Q|_+ + C1_{|Q|_+}(R_c\dot{Q} + L\ddot{Q}) \qquad (23)$$

where $1_{|Q|_+}(t) = 1$ when $Q > 0$ and else $1_{|Q|_+}(t) = 0$. $P_{\rm sv}$ is the systemic venous pressure, R_c the resistance due to aortic or pulmonary valve, R_p the peripheral resistance in the systemic or pulmonary circuit, C the arterial compliance and L the blood inertance. The right-hand side of (23) is nonzero only during the ejection, i.e. $Q > 0$. In Fig. 8, the arrows for C and R_p indicate these quantities can be functions of $P_{\rm ar}$.

For each ventricle Q being given by $Q = f(P_{\rm v}, P_{\rm ar}, P_{\rm at})$, Eq. (23) means that the derivative of the displacement for the intraventricular cavity has to be calculated up to the third order. Since the mechanical model has few inertia and damping, such a calculus is numerically hardly accessible and we neglect the inertance i.e. $L = 0$ in Eq. (23). For the left and right ventricle Eq. (23) is respectively written under the form

$$\dot{P}_{\rm ao} = W(P_{\rm ao}, P_{\rm lv}, P_{\rm sv}, P_{\rm at,l}) \quad \text{and} \quad \dot{P}_{\rm ap} = W(P_{\rm ap}, P_{\rm rv}, P_{\rm sv}, P_{\rm at,r})$$

the parameters could be different for each Windkessel model.

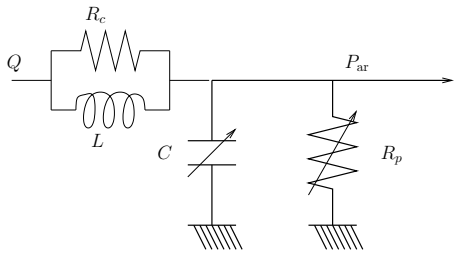

Figure 8: The 4-element Windkessel model.

2.5.4 The atria

We focus on the modelling of the two ventricles. The atria which allow to fill the ventricles during the diastole are not considered and we only assume that a low blood pressure P_{at} in each atriun allows the filling of the ventricles. Thus the atrial contraction at the end of the diastolic phase is not taken into account and one has

$$\dot{P}_{\mathrm{at,l}} = 0 \quad \text{and} \quad \dot{P}_{\mathrm{at,r}} = 0.$$

Even if the ventricle state – the initial stretching of the cardiac myocytes – prior to contraction is determined by the preload i.e. the atrium pressure, the atrial contraction (at resting heart rates) normally has little influence on ventricular preload and the most significant effect is created by the pressure drop in the ventricle due to passive relaxation thus most ventricular filling is passive. However, at high heart rates, enhanced atrial contractility (due to sympathetic activation) will play a significant role in ventricular filling and in determining preload. Note that to obtain more complex behavior, the modelling of the atrial contraction could be achieved using a 0D model.

2.6 Boundary conditions

The boundary conditions used for the structure take into account the two following phenomena

- the base of the myocardium is fastened to the arteries and the veins,
- the apex of the myocardium is almost still along a cardiac cycle whereas the base moves.

The previous requirements are satisfied using springs and dashpots located at the top end of the mesh, see Fig. 9-a. Moreover a translation of the muscle

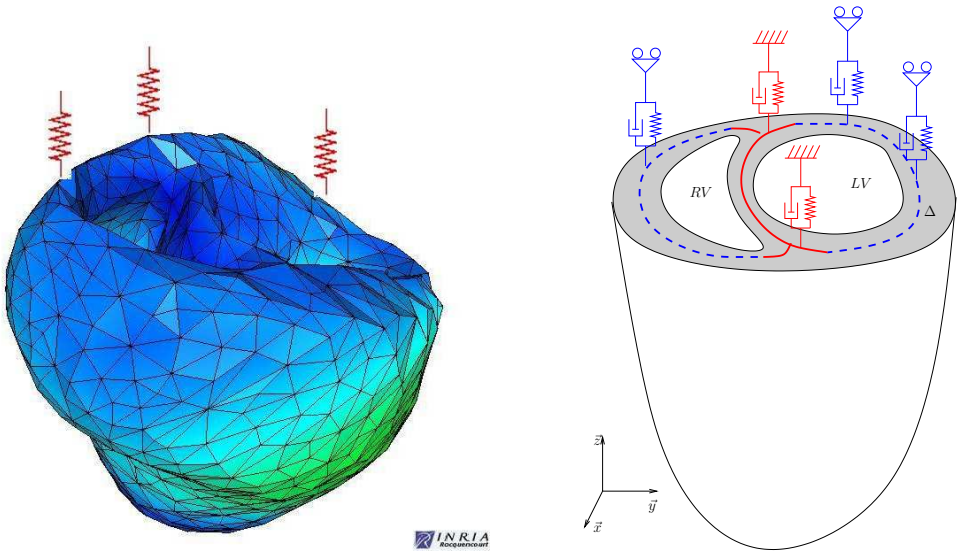

Figure 9: Springs and dashpots fastening the myocardium.

displacements ensures the apex is still. Note however, that this is only a post-processing of the results.

Let us consider a point A belonging to the curve Δ (solid part) of Fig. 9-b, if $\underline{A}^{(t)}$ denotes the position of A at time t then the force acting on A is

$$\underline{F}^A = k(\underline{A}^{(0)} - \underline{A}^{(t)}) - c\dot{\underline{A}}^{(t)}.$$

The velocity term $\dot{\underline{A}}^{(t)}$ is discretized as $\dot{\underline{A}}^{(t)} \approx \frac{1}{\Delta t}(\underline{A}^{(t)} - \underline{A}^{(t-1)})$.

Now if one considers a point B belonging to the dashed part of Δ, it is necessary to allow B to have displacements in directions $\vec{x}$ and $\vec{y}$ especially during ejection and filling phases. So the force acting on B has the expression

$$\underline{F}^B = k\Pi_z(\underline{B}^{(0)} - \underline{B}^{(t)}) - c\Pi_z\dot{\underline{B}}^{(t)}$$

Π_z being the projection on the $\vec{z}$ axis.

2.7 Initial conditions

Appropriate initial conditions need be prescribed. We consider the initial time t_0 corresponds to the end of the filling i.e. $Q = -\dot{V} = 0$ and $u \equiv 0$.

In practice, the initial conditions are difficult to estimate. For the simulations, we start with realistic initial values for the displacement $y(M, t_0) = y_0(M)$, the strain $\varepsilon(M, t_0) = \varepsilon_0(M)$, the strain in the contractile element $\varepsilon_c(M, t_0) = \varepsilon_{c,0}(M)$, the stiffness and the stress in the contractile element $k_c(M, t_0) = k_{c,0}(M)$, $\tau_c(M, t_0) = \tau_{c,0}(M)$. Since the system is supposed to have reached a static equilibrium, we also have $P_{\mathrm{v}}(t_0) = P_{\mathrm{at}}(t_0)$.

It has to be noticed that the system is periodic and rapidly reaches an attractor (limit cycle), whether after initialization or a modification of the parameters. Thus the initial conditions are "forgotten" by the system after a few cycles, see section 4.

2.8 Geometrical model

The geometric model used for the simulations (Fig. 10) comes from the Bio-Engineering Institute (Auckland university) and contains the cardiac fibre directions. The mesh has been refined using a surface mesh refinement (YAMS) and a 3D automatic mesh generation (GHS3D), both tools being developed by the INRIA team GAMMA.

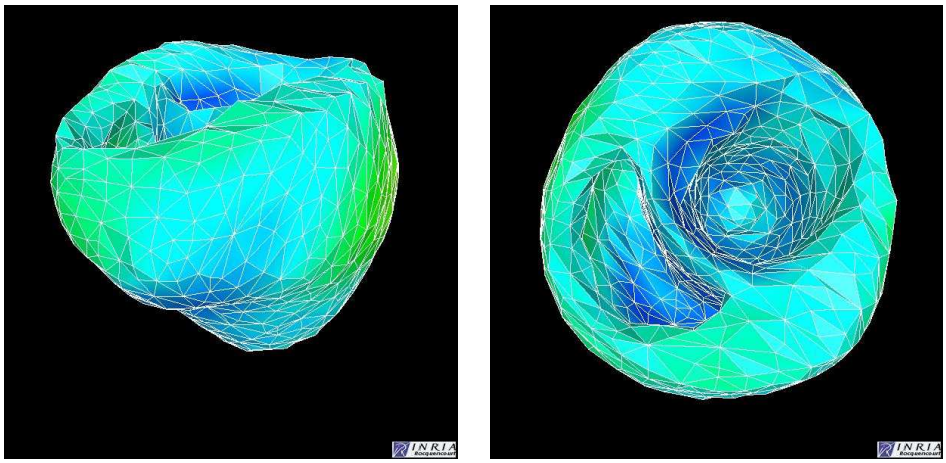

Figure 10: Mesh of the heart.

To each point of the mesh corresponds a vector giving the cardiac fibre direction at this point, see Fig. 11.

Due to the shape of the myocardium mesh, in order to be able to speak of the volume for each cavity, see Fig. 12-a, it is necessary to modify the available mesh to close each intraventricular cavity. Let us define for each ventricle

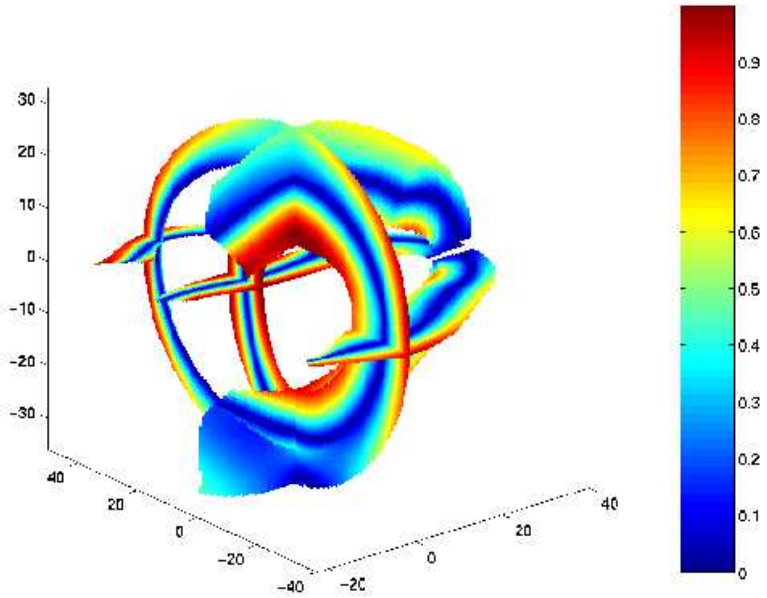

Figure 11: Cosine of the angle between the fibre direction and the apex-base axis.

$\partial\Gamma_O^{(t)}$, the contour line of $\Gamma_O^{(t)}$ and $B_{\Gamma_O^{(t)}}$ the barycenter of the points of the mesh drawing up the curve $\partial\Gamma_O^{(t)}$, see Fig. 12-a. Then we add to the initial mesh, tetrahedra built using point $B_{\Gamma_O^{(t)}}$ and the points of the contour line $\partial\Gamma_O^{(t)}$, see Fig. 13.

3 Discretization of the 3D problem

Assembling the modelling previously presented for the contractile fibres, the muscle matrix, the valve opening and closure, the arteries, the atria, we

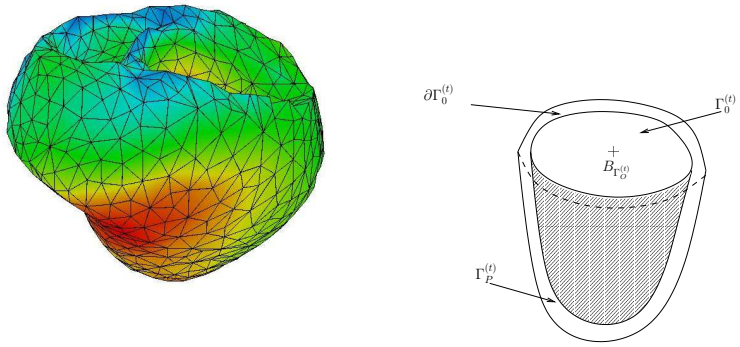

(a) *(b)*

Figure 12: *(a)* the geometrical model and *(b)* interior of a ventricular cavity (valid for the left and right ventricle), definition of $\Gamma_P^{(t)}$ and $\Gamma_O^{(t)}$.

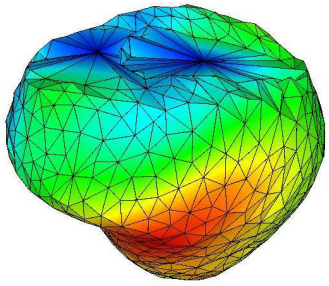

Figure 13: "Closed" mesh of the myocardium.

obtain the following formulation

$$(P)\ \begin{cases} \rho\ddot{\underline{y}} - \mathrm{div}(\underline{\underline{F}} \,.\, \underline{\underline{\sigma}}) = 0 \\ \underline{\underline{\sigma}} = \sigma_{1D}\ \underline{n} \otimes \underline{n} + E_p(\underline{\underline{\varepsilon}}) \\ \sigma_{1D} = \frac{\sigma_c}{1+\varepsilon_s} = \frac{\sigma_s}{1+\varepsilon_c} \\ \dot{\tau}_c = k_c\dot{\varepsilon}_c - (\alpha|\dot{\varepsilon}_c| + |u|)\tau_c + \sigma_0|u|_+ \\ \dot{k}_c = -(\alpha|\dot{\varepsilon}_c| + |u|)k_c + k_0|u|_+ \\ \sigma_c = d(\varepsilon_c)(\tau_c + k_c\xi_0) + \mu_c\dot{\varepsilon}_c \\ \sigma_s = E_s[(\varepsilon_{1D} - \varepsilon_c)/(1+\varepsilon_c)] \\ \varepsilon_{1D} = \sum_{i,j} E_{ij}n_in_j \\ -\dot{V}_{\mathrm{lv}} = f(P_{\mathrm{lv}}, P_{\mathrm{ao}}, P_{\mathrm{at,l}}) \\ -\dot{V}_{\mathrm{rv}} = f(P_{\mathrm{rv}}, P_{\mathrm{ap}}, P_{\mathrm{at,r}}) \\ \dot{P}_{\mathrm{ao}} = W(P_{\mathrm{ao}}, P_{\mathrm{lv}}, P_{\mathrm{sv}}, P_{\mathrm{at,l}}) \\ \dot{P}_{\mathrm{ap}} = W(P_{\mathrm{ap}}, P_{\mathrm{rv}}, P_{\mathrm{sv}}, P_{\mathrm{at,r}}) \\ \dot{P}_{\mathrm{at,l}} = 0 \\ \dot{P}_{\mathrm{at,r}} = 0 \\ \dot{P}_{\mathrm{sv}} = 0. \end{cases} \tag{24}$$

3.1 Formulation of deformation problem

Let us denote by $\Omega^{(t)}$ the domain occupied by the heart tissue at time t, by $\Gamma^{(t)} = \Gamma_P^{(t)} \cup \Gamma_O^{(t)}$ (see Fig. 12-b) the surface of the ventricular cavity, by $V^{(t)}$ a suitable space of admissible displacements and by V_0 the space of displacement test functions, cf. [8]. In the context of total Lagrangian formulation, the overall dynamic equilibrium and valve equations read

$$\int_{\Omega^{(0)}} \rho\ddot{\underline{y}}^{(t)} \cdot \underline{v}\mathrm{d}\Omega^{(0)} + \int_{\Omega^{(0)}} S_{ij}\delta E_{ij}\mathrm{d}\Omega^{(0)} + \int_{\Gamma^{(0)}} P_{\mathrm{v}}^{(t)}F_{ki}^{-1}n_k^{(0)}v_i\mathrm{d}\Gamma^{(0)} = 0 \quad \forall \underline{v} \in V_0 \tag{25}$$

$$-\dot{V}^{(t)} = f(P_{\mathrm{v}}^{(t)}, P_{\mathrm{ar}}^{(t)}, P_{\mathrm{at}}^{(t)}) = 0\ , \tag{26}$$

where $\delta E_{ij}(\underline{y};\underline{v}) = \frac{1}{2}(v_{i,j} + v_{j,i} + y_{k,i}v_{k,j} + y_{k,j}v_{k,i})$ and F_{ij}^{-1} are components of F^{-1}. Note that P_{v}, the pressure in each heart ventricle is a scalar constant. We have also approximated $\dot{V}$, the volume of each ventricle defined in (22) by $(V^{(t)} - V^{(t-1)})/\Delta t$. The cavity volume is obtained using the surface integral

$$V^{(t)} = \frac{1}{3}\int_{\Gamma^{(t)}} x_in_i^{(t)}\mathrm{d}\Gamma^{(t)} = \frac{1}{3}\int_{\Gamma^{(0)}} \delta_{ij}F_{ki}^{-1}n_k^{(0)}x_j\mathrm{d}\Gamma^{(0)}\ , \tag{27}$$

where $\underline{x} = \underline{X} + \underline{y}$ are the updated coordinates.

The deformation problem is completed by proper initial and boundary conditions as described in paragraphs 2.6, 2.5 and 2.7. We use, for example, the assumption of the static equilibrium at the initial time.

3.2 Time and space discretization

The equilibrium equation (25) is time-discretized using the Newmark scheme. Other equations with time rates (e.g. (8)) are discretized using a mid-point scheme i.e.

$$(\cdot)^{n+\frac{1}{2}} \approx ((\cdot)^n + (\cdot)^{n+1})/2$$
$$\dot{(\cdot)}^{n+\frac{1}{2}} \approx ((\cdot)^{n+1} - (\cdot)^n)/\Delta t.$$

This leads to the nonlinear problem in $\underline{y}$, ε_c and $P_{\rm v}$ for each time step. Note that ε_c (the deformation of the contractile element) is evaluated at the Gauss points and can develop independently on $\underline{y}$ because of the series elastic element.

For the discretization of space we use the finite element method. The discrete nonlinear systems of each time step are solved by the Newton method. The tangent linear system exhibits the following structure:

$$\begin{pmatrix} \mathbf{K_{11}} & \mathbf{K_{12}} & \mathbf{\Pi_1} \\ \mathbf{K_{21}} & \mathbf{K_{22}} & \mathbf{0} \\ \mathbf{\Pi_2} & \mathbf{0} & \Pi_3 \end{pmatrix} \begin{pmatrix} \mathbf{\Delta y} \\ \mathbf{\Delta \varepsilon_c} \\ \Delta P_{\rm v} \end{pmatrix} = \begin{pmatrix} \mathbf{f} \\ \mathbf{g} \\ h \end{pmatrix}, \tag{28}$$

where $\mathbf{f}$ is a discretized version of (25), $\mathbf{g}$ follows from (8)

$$g := \sigma_c - \sigma_s \frac{1+\varepsilon_c}{1+\varepsilon_s} = 0$$

and h corresponds to a discretization of (26). If the Windkessel model presented in paragraph 2.5.3 is used for each ventricle, the arterial pressures $P_{\rm ao}$ and $P_{\rm ap}$ are included in the state vector becoming $(\mathbf{y}, \varepsilon_\mathbf{c}, \mathbf{P})^\mathbf{T}$ where $\mathbf{P} = (\mathbf{P}_{\rm v}, \mathbf{P}_{\rm ao}, \mathbf{P}_{\rm ap})^\mathbf{T}$ is now a vector of pressure variables and $\mathbf{\Pi_3}$ is a matrix. The same holds for the case when only a ventricle is coupled with a Windkessel model with, e.g. for the left ventricle, $\mathbf{P} = (\mathbf{P}_{\rm v}, \mathbf{P}_{\rm ao})^\mathbf{T}$ and $\dot{P}_{\rm ap} = 0$.

To solve (28) we exploit the structure of $\mathbf{K_{22}} := \frac{\partial \mathbf{g}}{\partial \varepsilon_\mathbf{c}}$ which is diagonal and thus $\varepsilon_\mathbf{c}$ can be easily eliminated. Although $\Pi_3 := \frac{\partial h}{\partial P_{\rm v}}$ is also diagonal, it is not eliminated since its Schur complement $\mathbf{\Pi_1 \Pi_3}^{-\mathbf{1}} \mathbf{\Pi_2}$ would change the pattern of nonzeros of $\mathbf{K_{11}}$, leading to time-demanding memory reallocations. Hence we solve

$$\begin{pmatrix} \mathbf{K_{11}} - \mathbf{K_{12}K_{22}}^{-\mathbf{1}}\mathbf{K_{21}} & \mathbf{\Pi_1} \\ \mathbf{\Pi_2} & \Pi_3 \end{pmatrix} \begin{pmatrix} \mathbf{\Delta y} \\ \Delta P_{\rm v} \end{pmatrix} = \begin{pmatrix} \mathbf{f} - \mathbf{K_{12}K_{22}}^{-\mathbf{1}}\mathbf{g} \\ h \end{pmatrix} \tag{29}$$

by an unsymmetric multifrontal solver (UMFPACK package [11]), followed by

$$\mathbf{\Delta}\varepsilon_{\mathbf{c}} = \mathbf{K_{22}}^{-1}(\mathbf{g} - \mathbf{K_{21}}\mathbf{\Delta y}) \; . \tag{30}$$

Then we update the Newton iterates by $\mathbf{y} \leftarrow \mathbf{y} - \mathbf{\Delta y}$, $\varepsilon_{\mathbf{c}} \leftarrow \varepsilon_{\mathbf{c}} - \mathbf{\Delta}\varepsilon_{\mathbf{c}}$, $P_{\mathrm{v}} \leftarrow P_{\mathrm{v}} - \Delta P_{\mathrm{v}}$.

3.3 Time discretization of the windkessel model

Further let $Q^{(t)}$ be identified with $f(P_{\mathrm{v}}^{(t)}, P_{\mathrm{at}}^{(t)}, P_{\mathrm{ar}}^{(t)})$. Then for each ventricle we use

$$-\dot{V}^{(t+\frac{\Delta t}{2})} \approx -\frac{V^{(t+\Delta t)} - V^{(t)}}{\Delta t} = Q^{(t+\frac{\Delta t}{2})} \approx \frac{Q^{(t+\Delta t)} + Q^{(t)}}{2} \; ,$$

leading to the first equation to be satisfied:

$$V^{(t+\Delta t)} - V^{(t)} + \frac{\Delta t}{2}(Q^{(t+\Delta t)} + Q^{(t)}) = 0 \; . \tag{31}$$

Equation (23) is also discretized using the mid-point scheme

$$\dot{Q}^{(t+\frac{\Delta t}{2})} \approx \frac{Q^{(t+\Delta t)} - Q^{(t)}}{\Delta t} \; , \quad \dot{P}_{\mathrm{ar}}^{(t+\frac{\Delta t}{2})} \approx \frac{P_{\mathrm{ar}}^{(t+\Delta t)} - P_{\mathrm{ar}}^{(t)}}{\Delta t} \; ,$$

which leads to

$$P_{\mathrm{ar}}^{(t+\Delta t)} - P_{\mathrm{ar}}^{(t)} + \frac{\Delta t}{C}\left(\frac{\frac{1}{2}(P_{\mathrm{ar}}^{(t+\Delta t)} + P_{\mathrm{ar}}^{(t)}) - P_{\mathrm{sv}}}{R_p} - \left((1 + \frac{R_c}{R_p})|\frac{Q^{(t+\Delta t)} + Q^{(t)}}{2}|_+ + \frac{CR_c}{\Delta t}(|Q^{(t+\Delta t)}|_+ - |Q^{(t)}|_+)\right)\right) = 0 \; . \tag{32}$$

At $t = t_0$ we assume a steady state, where $P_{\mathrm{ar}} = 70$ mmHg and thus $Q^{(0)} = 0$.

3.4 Numerical behavior

In the simulations presented hereafter, the time step is constant with $\Delta t = 2$ ms. A correct simulation of each isovolumetric phase whose length is roughly 50 ms imposes that the time step does not overstep a limit (arround 5 ms). This constraint can be, to some extent, relaxed during ejection and filling so a adapative time step procedure could be introduced.

The simulations carried out have shown the global damping coming from the pseudo-potential W^v and the inertia term $\rho\ddot{y}$ have little influence compared to other internal forces.

4 Simulations

4.1 Calibration of the 3D model

A correct calibration of all the parameters appearing in the model is very important in order to obtain realistic simulations. The parameters to calibrate can be divided into three groups:

- the parameters used in the arteries models can be found in the litterature see especially the works of Stergiopulos *et al.* [35, 39] and the references therein.
- The unknow quantities appearing in the contraction constitutive law (2), mainly k_0 and σ_0 can be estimated easily since they represent the asymptotic value for k_c and τ_c respectively that can be found in the litterature e.g. [40].
- Concerning the calibration of the passive behavior of cardiac fibres, the available data e.g. in [38] and [32] are not in agreement and deal with general soft tissues but not typically the myocardium.

4.2 Simulations results (3D model)

We present some results of simulation carried out with model (24), animated versions of these results can be seen on the WEB site of the MACS project, see `www-rocq.inria.fr/MACS/Coeur/index.html`.

The presented results have been obtained after a simulation of several cardiac cycles so the approximate initial conditions are of no significance. Fig. 15 represents some classical indicators characteristic of the cardiac function. From left to right: left ventricle volume variations, blood pressure variations, PV cycle, aortic flow, mitral flow, contractile stress for a given point of the myocardium. Fig. 16 illustrates the Starling effect. Two PV cycles obtained with two different mitral pressures are plotted and the stroke volume increases with the mitral pressure.

Furthermore, the stability of the model is demonstrated by results obtained over a sequence of cycles, which show that the system rapidly reaches an attractor (limit cycle), whether after initialization or a modification of the parameters, see Fig. 14.

We also present simulations results representing pathological cases. We have considered that the contraction parameters k_0 and σ_0 were reduced in a given

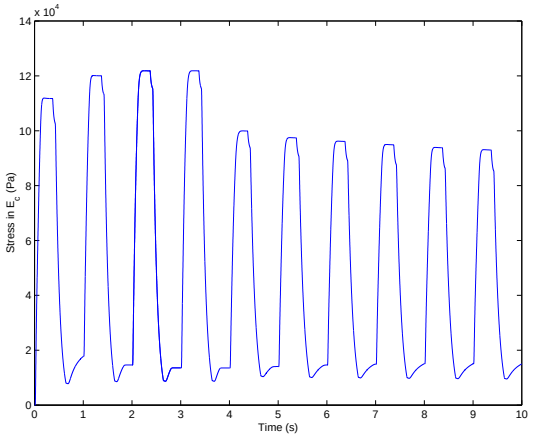

Figure 14: Stress σ_{1D} in a fibre over 10 cycles; a modification of σ_0, k_0 and u is introduced before the fourth cycle.

area of the myocardium, see Fig. 17. The stresses ans strains at the end of the ejection are first presented in Fig. 18. It is to be noticed that the kinematics of the muscle are only slightly modified by the variations of k_0 ans σ_0. The global indicators of the cardiac function for the pathological case but also for a reference situation are presented in Fig. 19.

5 Data assimilation

5.1 What is data assimilation ?

The aim of data assimilation is to incorporate measurements into a dynamical system model in order to produce accurate estimates of the current – and possibly future– state, parameters, initial conditions and input of the model.

To produce an accurate simulation or prediction using a model, precise knowledge of the considered phenomenon (boundary and initial conditions, parameters) is needed. This is achieved by using measurements and assimilating those observations into the model. In meteorology and oceanography, thousands of measurements are received in real time from a variety of captors e.g. satellites, aircraft, ships and land stations. Concerning muscle mechanics, the observation measurements are scarce in space and time and noisy so the set of quantities to estimate has to be chosen carefully and its size ought to be realistic with respect to the available measurements.

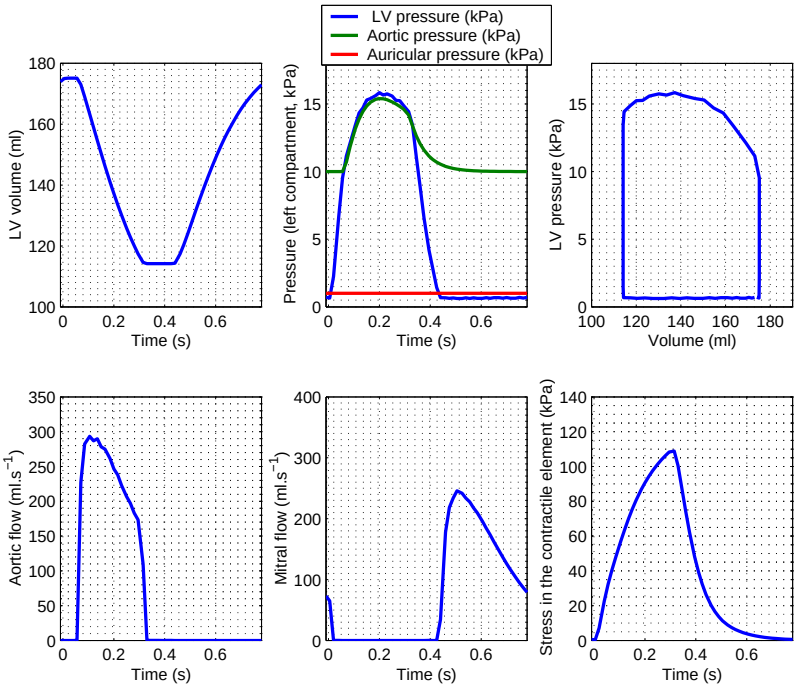

Figure 15: Global indicators of cardiac function.

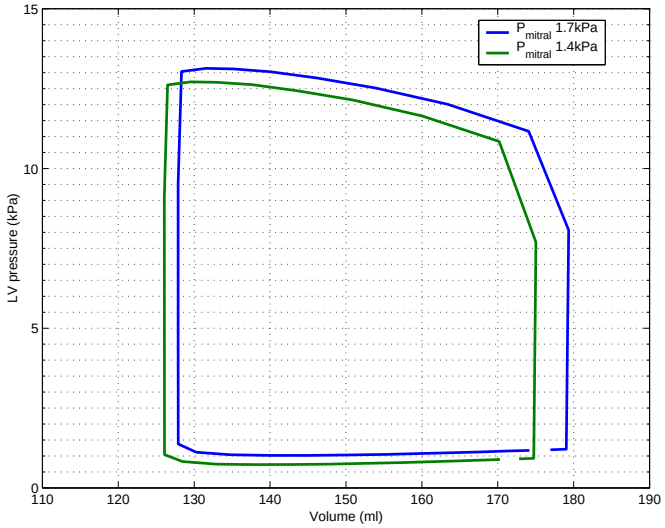

Figure 16: PV cycle for 2 different mitral pressures.

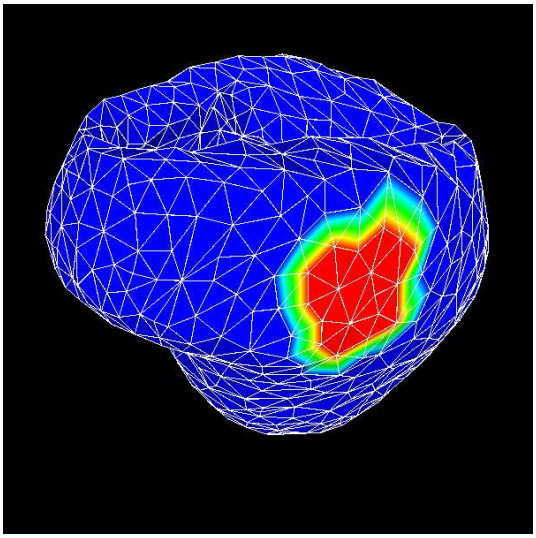

Figure 17: Area where the contractility is reduced (in red).

Without any model, the available measurements are often insufficient to determine the state of the considered system. So if one wants a detailed complete picture, we need additional information. Assimilation is the process of finding the model representation which is most consistent with the measurements. Data assimilation has been widely used in various forms in meteorological and oceanographic modelling since the 1950's. The various forms use ideas from different branches of mathematics e.g. probability, optimization and control theory.

H being the observation operator, $Y(t)$ the available measurements and $X(t)$ the model response, the general objective of the data assimilation is the minimization of the cost function i.e.:

$$J = \int_I \|Y(t) - HX(t)\|_\Omega^2 dt + penalty$$

that is performed over the set of variables to estimate (state, parameters,...), $\|.\|_\Omega$ is a suitable norm associated with the problem formulation. If I denotes the complete simulation time interval $[t_0, T]$, the assimilation technique is said to be variational and corresponds to an optimal control problem, see e.g. [36, 9, 25, 27]. By contrast if at each time step t_k, $I = [t_0, t_k]$, then the filtering technique is said to be sequential. This approach has been introduced by Kalman in the 1960's [19, 20] and widely used in various domains [23, 21, 7].

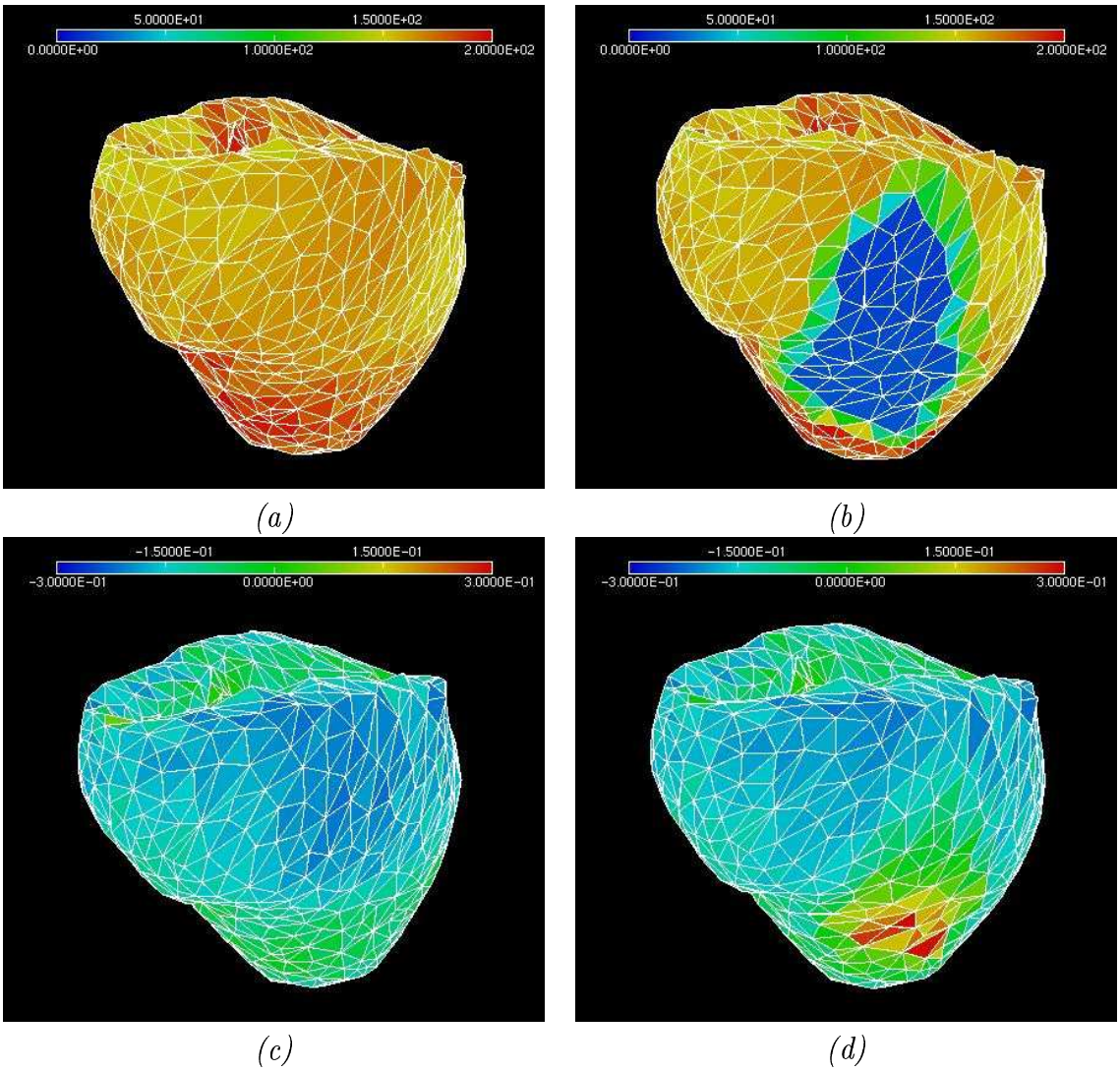

Figure 18: *(a)*, *(b)* Stress σ_c in kPa (end systole) and *(c)*, *(d)* Strain ($\|\varepsilon_c\|$) (end systole), left column: reference situation and right column pathological case.

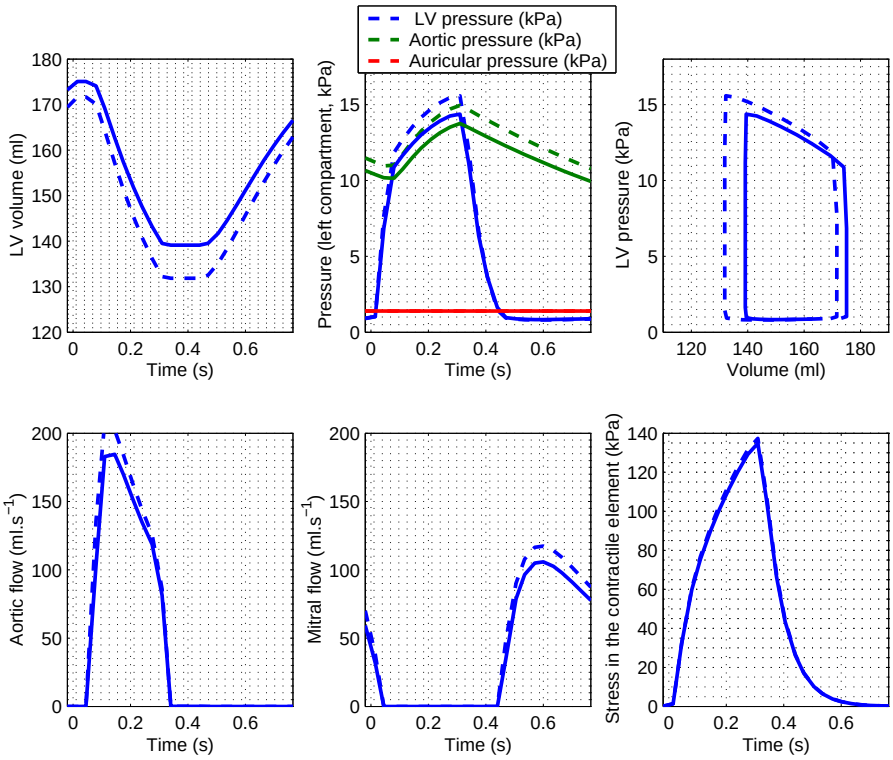

Figure 19: Global indicators of cardiac function (solid line: pathologic case, dashed line: reference case). The stress σ_c corresponds to a fibre in the neighbourhood of the ischemic area.

5.2 Numerical tests

Due to the complexity of the model and to observability considerations it is not possible to estimate all the quantities appearing in problem (24). Thus we focus on some of these parameters that are especially crucial for medical purposes in order to detect activation and contraction troubles, namely the parameters σ_0 and k_0. But even if the electrical activity modeling is not considered in this study, we are interested in the estimation of the electrical activity only from displacements measurements of the myocardium. Finally we are interested in the estimation of parameters k_0, σ_0 and input u from the available measurements.

The numerical validation of the sequential and variational data assimilation techniques are in progress. The results presented here have been obtained using numerically simulated observation measurements assimilated with the complete 3D problem (24) but over a simplified geometrical model depicted in Fig. 20.

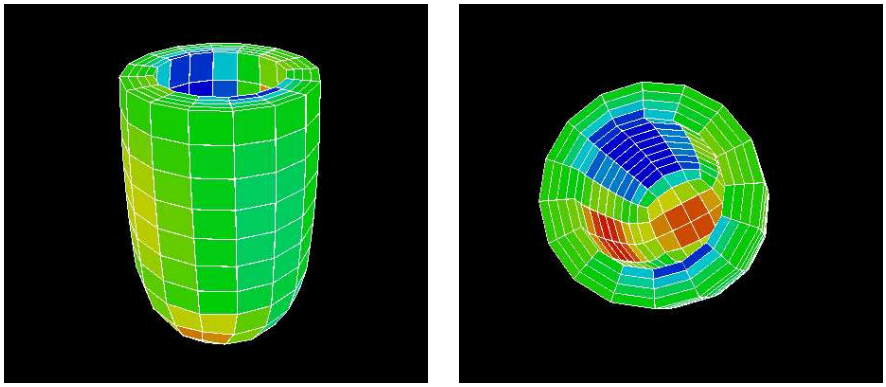

Figure 20: Simplified mesh used for the data assimilation ($\approx$ 900 nodes).

Both the sequential and variational techniques briefly described in paragraph 5.1 have been tested. Without considering the computational costs, the results given by the two methods are equivalent. The data assimilation process is the following:

- problem (24) is simulated with given input u and parameters k_0 and σ_0. Let us denote

$$X(M,t) = \begin{pmatrix} y(M,t) \\ \varepsilon_c(M,t) \\ \tau_c(M,t) \\ P(t) \end{pmatrix}$$

the obtained response of the model.

- The observations $\{Y(M_k, t_p)\}_{k,p}$ are obtained as follows

$$Y(M_k, t_p) = HX(M_k, t_p)$$

H being the chosen observation operator. Here we consider only displacements for points located at the epicardium and endocardium of the muscle are recorded.

- Starting from given input $\hat{u}$ and parameters $\hat{k}_0$ and $\hat{\sigma}_0$ different from the exact ones, the data assimilation is carried out. The objective is to obtain $\hat{u} \approx u$, $\hat{k}_0 \approx k_0$ and $\hat{\sigma}_0 \approx \sigma_0$. An example of estimation for σ_0 is given in Fig. 21, for this simulation we have considered the displacements at all the epicardium and endocardium nodes were known. We have also assumed $\sigma_0(M)$ is constant when M varies from the endocardium to the epicardium.

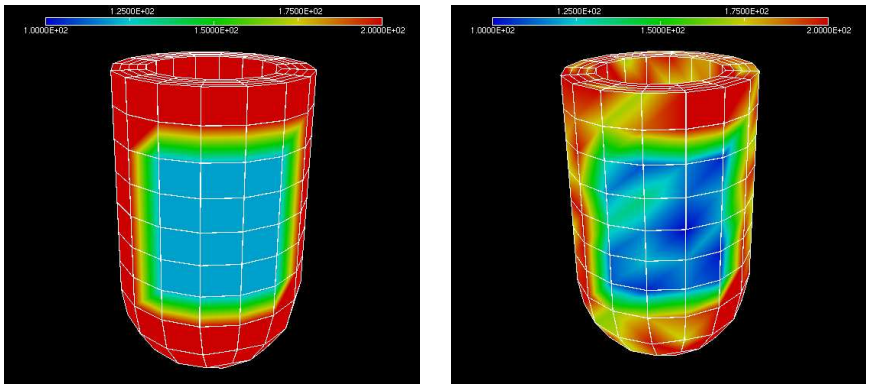

(a) *(b)*

Figure 21: *(a)* reference σ_0 and *(b)* its estimation using the variational technique.

6 Conclusion

We have proposed an electrically activated 3D mechanical model of the heart muscle. The modelling, the numerical implementation and the simulations are presented in this document. The main conclusion is that, even if more complete validations have to be carried out, our model seems to be able to

reproduce the actual behavior of a pathological or healthy heart. Concerning the 3D model, the works in progress are the following

- complete validation and calibration of the model,
- mathematical analysis of the model,
- data assimilation in 3D with real data,
- coupling with blood flow models (arteries and heart cavity).

We have also presented preliminary results concerning data assimilation techniques in order to detect activation and contraction troubles. Another objective is to estimate APD (action potential duration) and DT (depolarization time) from measurements of the mechanical activity synchronized by standard ECG. If this were possible, a complete estimation of the electrical traveling wave, useful to detect conductivity trouble, would be possible from the mechanical response of the sytem.

One of the major difficulties to be confronted in this approach lies in the conflict between the complexity of the model to be used (number of quantities to estimate) and the features (scarcity, quantities measured,...) of the measurements available in a clinical environment. Current techniques provide data on the electrical activity and the ventricular wall displacements. Even if the identification results presented here only used displacements measurements, in practice complementary data pertaining to stresses in the muscle or blood pressure – especially during isovolumetric phases – may be needed.

References

[1] Hodgkin A.L. and A.F. Huxley. A quantitative description of membrane current and its application to conduction and excitation in nerve. *J. Physiol.*, 177:500–544, 1952.

[2] R. Aliev and A.V. Panfilov. A simple two-variable model of cardiac excitation. *Chaos, Solitons and Fractals*, 7:293–301, 1996.

[3] A.P. Avolio. Multi-branched model of the human arterial system. *Med. Biol. Eng. Comput.*, 18(6):709–718, 1980.

[4] N. Ayache, D. Chapelle, F. Clément, Y. Coudière, H. Delingette, J.A. Désidéri, M. Sermesant, M. Sorine, and J. Urquiza. Towards model-based estimation of the cardiac electro-mechanical activity from ECG

signals and ultrasound images. In *Lectures Notes in Computer Science*, volume 2230. Eds T. Katila, I.E. Magnin, P. Clarysse, J. Montagnat, J. Nenonen, Springer-Verlag, 2001.

[5] J. Bestel, F. Clément, and M. Sorine. A biomechanical model of muscle contraction. In *Lectures Notes in Computer Science*, volume 2208. Eds W.J. Niessen and M.A. Viergever, Springer-Verlag, 2001.

[6] D. Chapelle, F. Clément, F. Génot, P. Le Tallec, M. Sorine, and J. Urquiza. A physiologically-based model for the active cardiac muscle. In *Lectures Notes in Computer Science*, volume 2230. Eds T. Katila, I.E. Magnin, P. Clarysse, J. Montagnat, J. Nenonen, Springer-Verlag, 2001.

[7] C.K. Chui and G. Chen. *Kalman Filtering With Real Time Applications.* Springer-Verlag., 1999.

[8] R. Cimrman. *Mathematical modelling of biological tissues.* PhD thesis, University of West Bohemia, Faculty of Applied Sciences, Department of Mechanics, 2002.

[9] P. Courtier and O. Talagrand. Variational assimilation of meteorological observations with the adjoint vorticity equation Part 1: Numerical results. *Quart. J. Roy. Meteorol. Soc.*, 113:1329–1347, 1987.

[10] O. Coussy. *Mechanics of porous continua.* Wiley, New-York, 1995.

[11] T. A. Davis. Algorithm 8xx: UMFPACK V4.1, an unsymmetric-pattern multifrontal method with a column pre-ordering strategy. Technical report, Univ. of Florida, CISE Dept., 2003. Also TR-03-007 at www.cise.ufl.edu/tech-reports.

[12] R.A. FitzHugh. Impulses and physiological states in theoretical models of nerve membranes. *Biophys. J.*, 1:445–466, 1961.

[13] Y.C. Fung. *Biomechanics: Mechanical Properties of Living Tissues.* Springer-Verlag, 2nd Ed., 1993.

[14] A.V. Hill. The heat of shortening and the dynamic constants in muscle. *Proc. Roy. Soc. London (B)*, 126:136–195, 1938.

[15] J.D. Humphrey. Continuum biomechanics of soft tissues. *Proc. R. Soc. Lond. A*, 459:3–46, 2002.

[16] P.J. Hunter, M.P. Nash, and G.B. Sands. Computational electromechanics of the heart. In *Computational biology of the heart*, pages 345–407. A.V. Panfilov and A.V. Holden Eds, John Wiley & Sons, 1997.

[17] A.F. Huxley. Muscle structure and theories of contraction. In *Progress in biophysics and biological chemistry*, volume 7, pages 255–318. Pergamon press, 1957.

[18] F. Jülicher, A. Ajdari, and J. Prost. Modeling molecular motors. *Reviews of Modern Physics*, 69(4), October 1997.

[19] R.E. Kalman. A new approach to linear filtering and prediction problems. *ASME Trans.–Journal of Basic Engineering*, 82(Series D):35–45, 1960.

[20] R.E. Kalman and R.S. Bucy. New results in linear ltering and prediction theory. *ASME Trans.–Journal of Basic Engineering*, 83(Series D):95–108, 1961.

[21] H. Kano, B.K. Ghosh, and H. Kanai. Single camera based motion and shape estimation using extended kalman filtering. *Math. Comput. Modelling*, 34(5-6):511–525, 2001.

[22] M. Kauer. *Inverse finite element characterization of soft tissues with aspiration.* PhD thesis, Swiss federal institute of techonology, 2001.

[23] B.P. Kellerhals. Financial pricing models in continuous time and Kalman filtering. *Lecture Notes in Economics and Mathematical Systems*, 506, 2001.

[24] A. Kolmogorov, I. Petrovsky, and N. Piscounoff. Etude de l'équation de la diffusion avec croissance de la quantité de matière et son application à un problème biologique. *Bull. Univ. Moscou Math, Serie Int. A*, 1:1–25, 1937.

[25] F.X. Le Dimet and O. Talagrand. Variational algorithms for analysis and assimilation of meteorological observation : theoretical aspects. *Tellus*, 38:97–110, 1986.

[26] D.H. Lin and F.C. Yin. A multiaxial constitutive law for mammalian left ventricular myocardium in steady-state barium contracture or tetanus. *J. Biomech. Eng.*, 120(4):504–517, 1998.

[27] J.L. Lions. *Contrôle optimal des systèmes gouvernés par des équations aux dérivées partielles.* Dunod, 1968.

[28] D.A. MacDonald. *Blood flow in arteries.* Edward Harold Press, 1974.

[29] I. Mirsky and W.W. Parmley. Assessment of passive elastic stiffness for isolated heart muscle and the intact heart. *Circul. Research*, 33:233–243, 1973.

[30] P.J. Mulquiney, N.P. Smith, K. Clark, and P.J. Hunter. Mathematical modelling of the ischaemic heart. *Nonlinear analysis*, 47:235–244, 2001.

[31] ICEMA (Images of Cardiac Electro-Mechanical Activity). WWW page `http://www-rocq.inria.fr/sosso/icema2/icema2.html`.

[32] D.P. Pioletti and L.R. Rakotomanana. Non linear viscoelastic laws for soft biological tissues. *Eur. J. Mech. A/Solids*, 19:749–759, 2000.

[33] D.P. Pioletti, L.R. Rakotomanana, J.F. Benvenuti, and Leyvraz P.F. Viscoelastic constitutive law in large deformations: application to human knee ligaments and tendons. *J. Biomech.*, 31:753–757, 1998.

[34] B.H. Smaill and P.J. Hunter. Structure and function of the diastolic heart: Material properties of passive myocardium. In *Theory of Heart: Biomechanics, Biophysics, and Nonlinear Dynamics of Cardiac Function.* Springer-Verlag, New-York, 1991.

[35] N. Stergiopulos, B.E. Westerhof, and N. Westerhof. Total arterial inertance as the fourth element of the windkessel model. *Am. J. Physiol.*, 276:H81–H88, 1999.

[36] O. Talagrand and P. Courtier. Variational assimilation of meteorological observations with the adjoint vorticity equation Part 1: Theory. *Quart. J. Roy. Meteorol. Soc.*, 113:1311–1328, 1987.

[37] C. Truesdell and W. Noll. *The non-linear filed theories of mechanics, 2nd ed.* Springer, Berlin, 1992.

[38] D.R. Veronda and R.A. Westmann. Mechanical characterization of skin - finite deformation. *Journal of Biomechanics*, 3:114–124, 1970.

[39] N. Westerhof, F. Bosman, C.J. De Vries, and A. Noordegraaf. Analog study of the human systemic arterial tree. *J. Biomech.*, 2:121–143, 1969.

[40] J.Z. Wu and W. Herzog. Modelling concentric contraction of muscle using an improved cross-bridge model. *Journal of Biomechanics*, 32:837–848, 1999.

[41] G.I. Zahalak. A distribution moment approximation for kinetic theories of muscular contraction. *Mathematical Biosciences*, 55:89–114, 1981.